Supporting information for

The Design and Investigation of Porphyrins with Liquid Crystal Properties at Room Temperature

Christopher J. Wilson[a], Daniela A. Wilson[a,b], Ross W. Boyle[a*], and Georg H. Mehl[a*]

[a]Department of Chemistry, University of Hull, Kingston-upon-Hull, East Yorkshire, HU6 7RX, UK
[b]Institute for Molecules and Materials, Radboud University Nijmegen, Heyendaalseweg 135, 6525 AJ, Nijmegen, The Netherlands.

Table of Contents

1.0 Experimental

1.1 Materials

All starting materials were purchased from Sigma Aldrich, with the exception of 4-hydroxy-4'-carbonitrilebiphenyl which was supplied by Merck KgaA chemicals. All chemicals were used as received, solvents were dried according to common laboratory methods, distilled under inert atmosphere and stored over 3Å molecular sieves. Pyrrole was distilled under an inert atmosphere before use. Dichloromethane was passed through a column of alumina to remove residual HCl prior to use.

1.2 Techniques

Thin-layer chromatography (TLC) was performed using Merck aluminium plates coated with silica gel 60 F_{254} and visualised using either bromine vapour, iodine vapour or under UV light. Gravity percolation chromatography was performed using Fluorochem Silica Gel 35-70 μm 60 Å or ICN Silica Gel 32-63 μm 60 Å. NMR spectra were recorded on a Jeol JNM ECP400 spectrometer, with TMS δ_H = 0 as the internal standard or residual protic solvent. [$CDCl_3$, δ_H = 7.26; C_6D_6, δ_H = 7.16; $(CD_3)_2SO$, δ_H = 2.50, $(CD_3)OD$, δ_H = 3.30]. Chemical shifts are given in ppm (δ) and coupling constants (*J*) are given in Hertz (Hz). ^1H NMR were recorded at 400 MHz; ^{13}C recorded at 100.5 MHz with the central peak of $CDCl_3$ (δ_C =77.0 ppm), as the internal reference. Mass spectra were recorded using either a Bruker Reflex IV matrix assisted laser desorption ionisation-time of flight (MALDI-TOF) mass spectrometer or a ThermoFinnigan LCQ Classic electrospray mass spectrometer. Samples analysed using MALDI-TOF were run in HABA matrix. Samples analysed by electrospray were directly loop injected through the inject/direct valve. Purity was determined using Viscotek Triple Detection GPC system comprising of -270 Dual detector with Viscometry and RALS (Right Angle Laser Light Scattering), VE3580 RI detector, VE1122 solvent pump, column oven and solvent degasser. Viscotek Omnisec 4.0 software. Set of 2 columns plus guard - TSKgel GMHHR-L(<10k mw) 5μm mixed bed 300 x 7.8mm. SKgel is a porous, highly crosslinked spherical polystyrene divinylbenzene resin. Conventional Calibration - used with RI detector only - calibrated with 10 polystyrene narrow standards to give polystyrene equivalent molecular weight values. UV-visible spectra were measured on an Agilent 8453 diode array spectrometer and Varian Cary 50 spectrophotometer. Differential scanning calorimetry was carried out using a Mettler DSC822e with STARe software

calibrated with indium (156.6°C 28.45J/g) and zinc (419.47°C), checked with indium ± 0.3, and Aluminium reference sample. OPM analysis and images were recorded using an Olympus BH2 polarising microscope, Mettler FP52 and FP82 heating stage and controller, Photography- JVC TK-C1481 colour video camera using Mettler Studio Capture software.

Powder X-ray diffraction (XRD) studies were performed on a MAR345 diffractometer, equipped with 2D image plate detector, CuK_α radiation source, graphite monochromator, λ = 1.541 Å. The background or diffraction peaks were fitted with polynomial, Gaussian, Lorentzian, Lorentzian squared or Voigt peak-shape fitting. FIT2D, DataSqueeze and Origin software packages were used for XRD data analysis.

Molecular modelling was performed using PCGamess (Firefly) modelling software. In all cases the molecular and supramolecular assemblies were minimised using PM6 algorithm.

2.0 Synthesis of mesogenic building blocks and liquid crystalline porphyrins

5,15-Di(11-undec-1-eneylphenyl) porphyrin (2) 5,15-(4-hydroxyphenyl)porphyrin (500 mg, 1.01 mmol) was dissolved in butanone along with 11-bromoundec-1-ene (704 mg 3.03 mmol). To this was added potassium carbonate (1.3 g 10 eq) and a catalytic amount of potassium iodide. The reaction was heated under reflux over night, after which the reaction was allowed to cool and filtered. The potassium carbonate was washed with copious amounts of hot butanone (50 mL portions), the filtrates were combined and the solvent removed under reduced pressure. The red brown residue was purified by flash chromatography (silica, eluent: DCM/Hexane 1:1). The relevant fractions were collected and concentrated, the product was precipitated by solvent exchange with hexane after filtration was re-dissolved in dichloromethane and the solvent removed to yield a shiny purple wax (200 mg 25%); Rf 0.43: λ_{max}(DCM)/nm 410, 503, 539, 576, 634; δ_H (400MHz; CDCl3; Me_4Si) -3.15 (2H, bs, N*H*), 1.41 (12H, m, CH_2), 1.65 (12H, m, CH_2), 2.0 (4H, m, CH_2), 2.1 (4H, m, CH_2), 4.26 (4H, d, J=6.2Hz O-CH_2), 5.03 (4H, ddt, J = 10.08Hz, J = 2.20Hz, J = 1.29Hz, Hc), 5.86 (2H, ddt, J = 17.23Hz, J = 2.20Hz, J = 1.29Hz, Hb), 7.31 (4H, d, J = 8.06Hz Ar2), 8.15 (4H, d, J = 8.06Hz Ar3), 9.09 (4H, d, J = 4.40Hz Beta-H), 9.36 (4H, d, J = 4.40Hz, Beta-H), 10.27 (2H, s, meso-H); δ_C (100MHz; CDCl3; Me_4Si) 26.350, 29.094, 29.304, 29.627, 29.734, 33.969, 68.452, 105.229, 113.178, 114.290, 119.041, 131.132,

131.578, 133.621, 135.981, 139.384, 145.169, 147.621, 159.162; m/z (MALDI) 798.5 (M^+); GPC 17.22 mL.

5,15-Di(-1,1,3,3-tetramethyl-disiloxane-1-(pentyl-5-oxy-4-biphenyl-4'-carbonitrile)-3-(undecyl-11-oxy-4-phenyl))porphyrin (5)

Compound **2** (200mg, 0.25mmol) was dissolved in dry toluene (15 mL) along with **4**[1] (250 mg, 0.63 mmol). Platinum(0)-1,1,3,4-tetramethyl-1,3-divinyldisiloxane (Karstedt's catalyst) was added (10-20 drops) and dried compressed air bubbled through the reaction mixture for 10 to 15 seconds. The reaction was protected from light and allowed to stir between 10-18°C for 12 hours. The solvent was then removed under reduced pressure and the residue was purified by flash chromatography (SiO_2 Eluent DCM and hexane mixture 2:1). Fractions were collected and analysed by TLC the relevant fractions were concentrated to yield the product as a purple wax in 50% yield (199 mg): λ_{max}(DCM)/nm 410, 505, 541, 578, 634; δ_H (400MHz; CDCl3; Me_4Si) -3.14 (2H, bs, NH), 0.07 (24H, m, Si-CH_3), 0.56 (8H, m, Si-CH2), 1.34 (16H, m, CH_2), 1.41 (12H, m, CH_2), 1.49 (8H, m CH_2), 1.64 (4H, q, CH_2), 1.81 (4H, q, CH_2), 2.00 (4H, q, J = 6.60Hz CH_2), 3.97 (4H, t, J = 6.60Hz O-CH_3), 4.27 (4H, t, J = 6.60Hz, O-CH_2), 6.94 (4H, d, J = 8.80Hz, Ar), 7.33 (4H, d, J = 8.60Hz, Porph-Ar), 7.44 (4H, d, J = 8.80Hz, Ar), 7.56 (4H, d, J = 8.60Hz, Ar), 7.61 (4H, d, J = 8.60Hz, Ar), 8.16 (4H, d, J = 8.60Hz, Porph-Ar), 9.10 (4H, d, J = 4.59Hz, Porph-Beta), 9.38 (4H, d, J = 4.59Hz, Porph-Beta), 10.29 (2H, s, Porph-Meso); δ_C (100MHz; CDCl3; Me_4Si) 0.92, -0.43, 17.94, 18.00, 22.73, 22.90, 25.84, 28.55, 29.04, 29.10, 29.14, 29.24, 29.29. 33.05, 67.70, 67.94, 104.70, 109.52, 112.65, 114.59, 118.50, 118.68, 126.55, 127.82, 130.59, 130.73, 131.50, 132.07, 133.08, 135.44, 144.62, 144.77, 144.09, 158.63, 159.34; m/z (MALDI) 1594.4 (M^+); GPC 15.37 mL.

5-(1,1,3,3-Tetramethyl-disiloxane-1-(pentyl-5-oxy-4-biphenyl-4'-carbonitrile)-3-(undecyl-11-oxy-4-phenyl))-15-(undec-2-eneyloxpheny)porphyrin (6) was isolated as a by-product from synthesis of **5** in 150 mg yield (40%): λ_{max}(DCM)/nm 410, 505, 541, 578, 634; δ_H (400MHz; CDCl3; Me_4Si) -3.08 (2H, bs, NH), 0.07 (12H, m, Si-CH_3), 0.56 (4H, m, Si-CH2), 0.92 (3H, m, CH_3) 1.35 (16H, m, CH_2), 1.41 (8H, m, CH_2), 1.51 (6H, m, CH_2), 1.68 (4H, m, CH_2), 1.81 (2H, m, CH_2), 2.04 (4H, m, CH_2), 3.98 (2H, t, J = 6.65Hz, O-CH_2), 4.28 (2H, t, J = 6.65Hz, O-CH_2), 4.29 (2H, t, J = 6.65Hz, O-CH_2), 5.47 (2H, m, CH), 6.96 (2H, d, J = 8.80Hz, Ar), 7.33 (2H, d, J = 8.80Hz, Ar), 7.34 (2H, d, J = 8.80Hz, Ar), 7.47 (2H, d, J = 8.80Hz, Ar), 7.57 (2H, d, J = 8.41Hz, Ar), 7.63 (2H, d, J = 8.41Hz, Ar), 8.17 (2H, d, J =

8.70Hz, Ar), 8.17 (2H, d, J = 8.70Hz, Ar), 9.11 (2H, d, J = 4.50Hz, Porph-Beta), 9.12 (2H, d, J = 4.50Hz, Porph-Beta), 9.39 (2H, d, J = 4.60Hz, Porph-Beta), 9.40 (2H, d, J = 4.60Hz, Porph-Beta), 10.30 (2H, s, Porph-Meso); δ_C (100MHz; CDCl3; Me_4Si) -0.43, 0.83, 17.94, 18.02, 22.73, 22.91, 25.84,28.56, 28.98, 29.04, 29.11, 29.14, 29.24, 29.28, 31.54, 33.00, 67.72, 67.90, 104,70, 109.54, 112.66, 114.61, 118.49, 118.54, 118.68, 126.56, 127.83, 130.59, 130.62, 130.75, 131.05, 132.08, 133.11, 135.43, 144.64, 144.79,147.10, 158.64, 159.36, 135.43; m/z (MALDI)1195.7(M^+); GPC 16.04 mL.

5,15-Di(-1,1,3,3-tetramethyl-disiloxane-1-(1-pentyl-5-oxy-4-biphenyl-4'-carbonitrile)-3-(1-undecyl-11-oxy-4-phenyl))porphyrinato Zinc (II) (**Zn(II)5**) Compound **Zn(II)2** (200 mg, 0.32 mmol) was dissolved in dry toluene (15 mL) along with **4**[1] (250 mg, 0.63 mmol). Platinum(0)-1,1,3,4-tetramethyl-1,3-divinyldisiloxane (Karstedt's catalyst) was added (10-20 drops) and dried compressed air bubbled through the reaction mixture for 10 to 15 seconds. The reaction was protected from light and allowed to stir between 10-18°C for 12 hours. The solvent was then removed under reduced pressure and the residue was purified by flash chromatography (SiO_2 Eluent DCM and hexane mixture 2:1). Fractions were collected and analysed by TLC the relevant fractions were concentrated to yield the product as a purple wax in 50% yield (192 mg): λ_{max}(DCM)/nm 411, 534; δ_H (400MHz; CDCl3; Me_4Si) 0.068 (24H, m, Si-CH_3), 0.56 (8H, m, Si-CH_2) 1.35 (16, m, CH_2), 1.41 (12H, m, CH_2), 1.50 (8H, m, CH_2), 1.65 (4H, q, J = 6.55, CH_2), 1.80 (4H, q, J = 6.55), 2.01 (4H, q, J = 6.55, CH_2), 3.96 (4H, t, J = 6.55Hz, O-CH_2), 4.28 (4H, t, J = 6.55Hz, O-CH_2), 6.92 (4H, d, J = 8.80Hz, Ar), 7.32 (4H, d, J = 8.60Hz, Porph-Ar) 7.43 (4H, d, J = 8.80, Ar), 7.54 (4H, d, J = 8.50Hz, Ar), 7.60 (4H, d, J = 8.50Hz, Ar), 8.15 (4H, d, J = 8.60Hz, Porph-Ar), 9.18 (4H, d, J = 4.50Hz, Porph-Beta), 9.43 (4H, d, J = 4.50Hz, Porph-Beta), 10.30 (2H, s, Porph-Meso); δ_C (100MHz; CDCl3; Me_4Si) -0.44, 0.92, 17.92, 18.00, 22.73, 22.90, 25.85, 28.53, 29.04, 29.11, 29.14, 29.24, 29.28, 29.30, 33.06, 67.69,67.92, 109.45, 112.27, 114.55, 118.67, 119.47, 126.51, 127.78, 130.67, 131.19, 132.05, 132.13, 134.30, 135.18, 144.73, 148.94, 150.04, 158.42, 159.03, 159.29; m/z (ESI) 1656.2(M^+); GPC 15.33 mL.

5-(1,1,3,3-Tetramethyl-disiloxane-1-(pentyl-5-oxy-4-biphenyl-4'-carbonitrile)-3-(undecyl-11-oxy-4-phenyl))-15-(undec-2-eneyloxpheny)porphyrinato Zinc(II) (**Zn(II)6**) was isolated as a by-product from the synthesis of **Zn(II)5** 154 mg (50%) : λ_{max}(DCM)/nm 411, 538; δ_H (400MHz; CDCl3; Me_4Si) 0.07 (12H, m, Si-CH_3), 0.56 (4H, m, Si-CH2), 0.92 (3H, m, CH3), 1.35 (16H, m, CH_2), 1.41 (8H, m, CH_2), 1.51 (6H, m, CH_2), 1.68 (4H, m,

CH_2), 1.81 (2H, m, CH_2), 2.04 (4H, m, CH_2), 3.96 (2H, t, J = 6.65Hz, O-CH_2), 4.28 (2H, t, J = 6.55Hz, O-CH_2), 4.29 (2H, t, J = 6.55Hz, CH_2), 5.47 (1H, m, CH), 5.49 (1H, m, CH), 6.93 (2H, d, J = 8.80Hz, Ar), 7.32 (2H, d, J = 8.80Hz, Ar), 7.33 (2H, d, J = 8.80Hz, Ar), 7.44 (2H, d, J = 8.80Hz, Ar), 7.54 (2H, d, J = 8.60Hz, Ar), 7.61 (2H, d, J = 8.60Hz, Ar), 8.15 (2H, d, J = 8.60Hz, Ar), 8.16 (2H, d, J = 8.60Hz, Ar), 9.18 (2H, d, J = 4.50Hz, Porph-Beta), 9.19 (2H, d, J = 4.50Hz, Porph-Beta), 9.44 (2H, d, J = 4.50Hz, Porph-Beta), 9.45 (2H, d, J = 4.50Hz, Porph-Beta), 10.32 (2H, s, Porph-Meso); δ_C (100MHz; CDCl3; Me_4Si) -0.44, 0.92, 17.92, 18.00, 22.73, 22.90, 25.85, 28.53, 29.04, 29.11, 29.14, 29.24, 29.28, 29.30, 31.54, 33.06, 67.69,67.92, 109.45, 112.27, 114.55, 118.54, 118.67, 119.47, 126.51, 127.78, 130.62, 130.67, 131.19, 132.05, 132.13, 134.30, 135.18, 144.73, 148.94, 150.04, 158.42, 159.03, 159.29; m/z (MALDI) 1257.6(M^+); GPC 16.17 mL.

5,15-Di(-1,1,3,3-tetramethyl-disiloxane-1-(1-pentyl-5-oxy-4-biphenyl-4'-carbonitrile)-3-(1-undecyl-11-oxy-4-phenyl))porphyrinato Nickel (II) (**Ni(II)5**) Compound **Ni(II)2** (200mg, 0.33mmol) was dissolved in dry toluene (15 mL) along with **4**[1] (250 mg, 0.63 mmol). Platinum(0)-1,1,3,4-tetramethyl-1,3-divinyldisiloxane (Karstedt's catalyst) was added (10-20 drops) and dried compressed air bubbled through the reaction mixture for 10 to 15 seconds. The reaction was protected from light and allowed to stir between 10 - 18°C for 12 hours. The solvent was then removed under reduced pressure and the residue was purified by flash chromatography (SiO_2 Eluent DCM and hexane mixture 2:1). Fractions were collected and analysed by TLC the relevant fractions were concentrated to yield the product as a purple wax in 50% yield (152 mg): λ_{max}(DCM)/nm 406, 516; δ_H (400MHz; CDCl3; Me_4Si) 0.05 (24H, m, $SiCH_3$), 0.55 (8H, m, $SiCH_2$), 1.33 (16H, m, CH_2), 1.40 (12H, m, CH_2), 1.49 (8H, m, CH_2), 1.60 (4H, m, CH_2), 1.81 (4H, m, CH_2), 1.97 (4H, m, CH_2), 3.97 (4H, t, J = 6.55Hz, O-CH_2), 4.22 (4H, t, J = 6.55Hz, O-CH_2), 6.94 (4H, d, J = 8.80Hz, Ar), 7.24 (4H, d, J = 8.80Hz, Ar), 7.45 (4H, d, J = 8.80Hz, Ar), 7.55 (4H, d, J = 8.60Hz, Ar), 7.62 (4H, d, J = 8.60Hz, Ar), 7.95 (4H, d, J = 8.80Hz, Ar), 8.97 (4H, d, J = 4.60Hz, Porph-Beta), 9.17 (4H, d, J = 4.60Hz, Porph-Beta), 9.91 (2H, s, Porph-Meso); δ_C (100MHz; CDCl3; Me_4Si) -0.44, 0.92, 18.47, 18.53, 23.26, 23.43, 26.34, 29.08, 29.56, 29.65, 29.76, 29.83, 33.58, 68.23, 68.41, 105.09, 110.02, 113.01,115.10, 118.24,119.23, 127.08, 128.35, 131.24, 131.99, 132.55, 132.60, 133.25, 134.96, 142.57, 143.34, 145.30, 159.07, 159.85; m/z (ESI) 1648.8 (M^+); GPC 15.46 mL.

5-(1,1,3,3-Tetramethyl-disiloxane-1-(pentyl-5-oxy-4-biphenyl-4'-carbonitrile)-3-(undecyl-11-oxy-4-phenyl))-15-(undec-2-eneyloxpheny)porphyrinato Nickel (II) (**Ni(II)6**) was isolated as a by-product from the synthesis of **Ni(II)5** yielding 150 mg of purple waxy solid (50%); λ_{max}(DCM)/nm 406, 516; δ_H (400MHz; $CDCl_3$; Me_4Si)
0.07 (12H, m, Si-CH_3), 0.56 (4H, m, Si-CH2), 0.92 (3H, m, CH3), 1.35 (16H, m, CH_2), 1.41 (8H, m, CH_2), 1.51 (6H, m, CH_2), 1.68 (4H, m, CH_2), 1.81 (2H, m, CH_2), 2.04 (4H, m, CH_2), 3.98 (2H, t, J = 6.55Hz, O-CH_2), 4.23 (2H, t, J = 6.55Hz, O-CH_2), 4.24 (2H, t, J = 6.55Hz, O-CH_2), 5.47 (2H, m, CH), 6.95 (2H, d, J = 8.80Hz, Ar), 7.23 (2H, d, J = 8.80Hz, Ar), 7.24 (2H, d, J = 8.80Hz, Ar), 7.46 (2H, d, J = 8.60Hz, Ar), 7.56 (2H, d, J = 8.60Hz, Ar), 7.62 (2H, d, J = 8.60Hz, Ar), 7.96 (2H, d, J = 8.60Hz, Ar), 7.96 (2H, d, J = 8.60Hz, Ar), 8.97 (2H, d, J = 4.50Hz, Porph-Beta), 8.98 (2H, d, J = 4.50Hz, Porph-Beta), 9.18 (2H, d, J = 4.79Hz, Porph-Beta), 9.18 (2H, d, J =4.79Hz, Porph-Beta), 9.92 (2H, s, Porph-Meso); δ_C (100MHz; $CDCl_3$; Me_4Si)
-0.44, 0.92, 18.47, 18.53, 23.26, 23.43, 26.34, 29.08, 29.56, 29.65, 29.76, 29.83, 31.54, 33.58, 68.23, 68.41, 105.09, 110.02, 113.01,115.10, 118.24, 118.54, 119.23, 127.08, 128.35, 130.62, 131.24, 131.99, 132.55, 132.60, 133.25, 134.96, 142.57, 143.34, 145.30, 159.07, 159.85; m/z (ESI) 1251.6 (M^+); 16.17 mL.

3.0 GPC Traces of Porphyrin Containing Materials

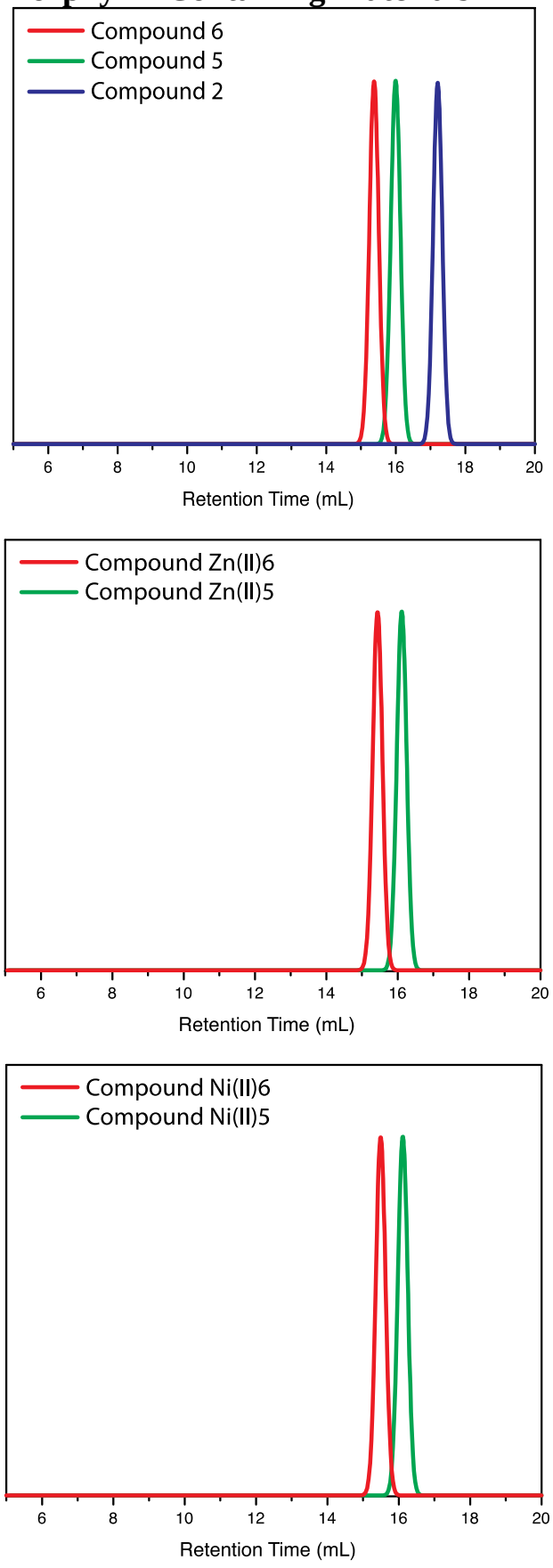

Supporting Figure 1. GPC traces for porphyrin containing materials

4.0 Differential Scanning Calorimetry Traces

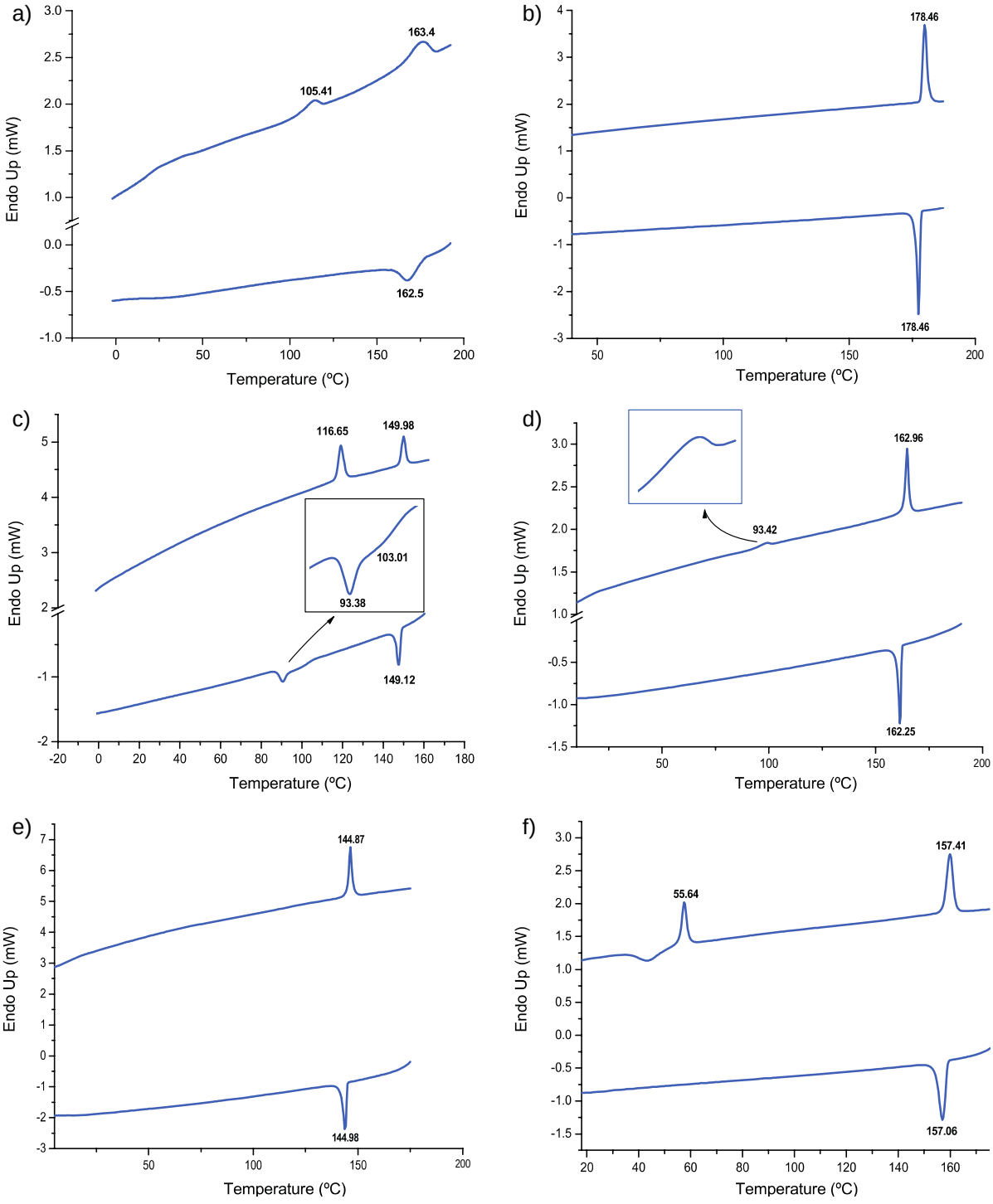

Supporting Figure 2. Differential scanning calorimetry plots for a) 5, b) 6, c) Zn(II)5, d) Zn(II)6, e) Ni(II)5, f) Ni(II)6.

5.0 Optical Polarising Microscopy

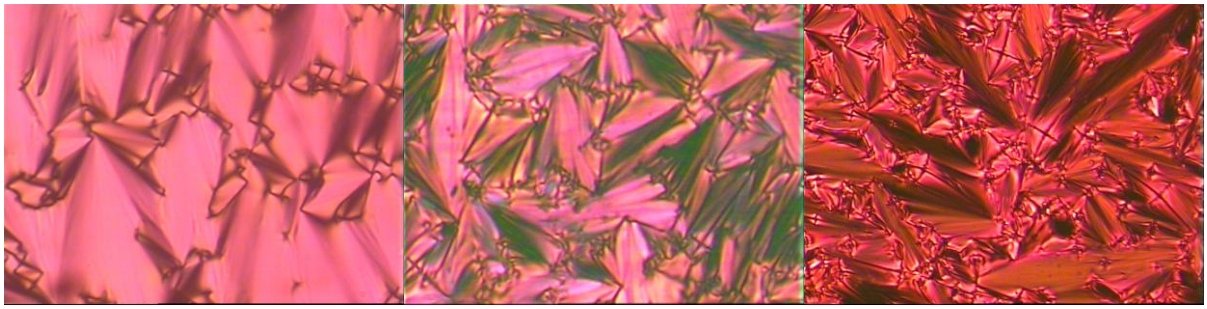

Supporting Figure 3. Optical polarising microscopy images **5 (**a) and **Zn(II)5** (b) at 20 °C, **Ni(II)5** (c) at 157 °C.

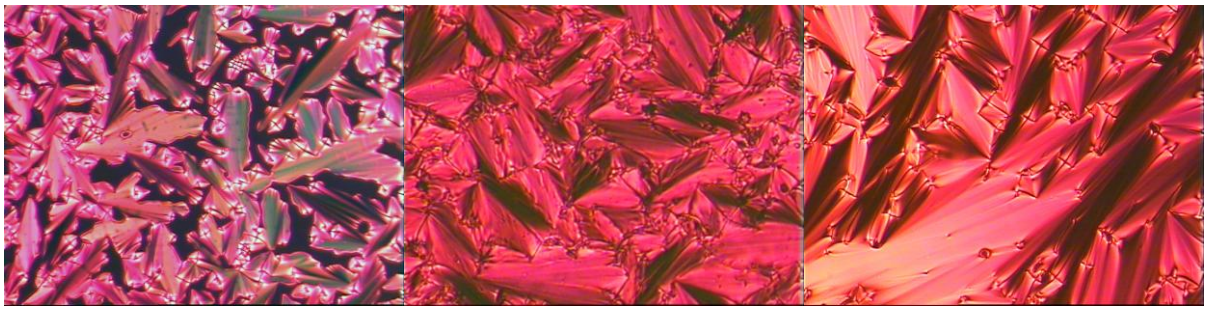

Supporting Figure 4. Optical polarising microscopy images **6 (**a) at 141 °C and 6-**Zn(II)** (b) at 141 °C, 6-**Ni(II)** (c) at 158 °C.

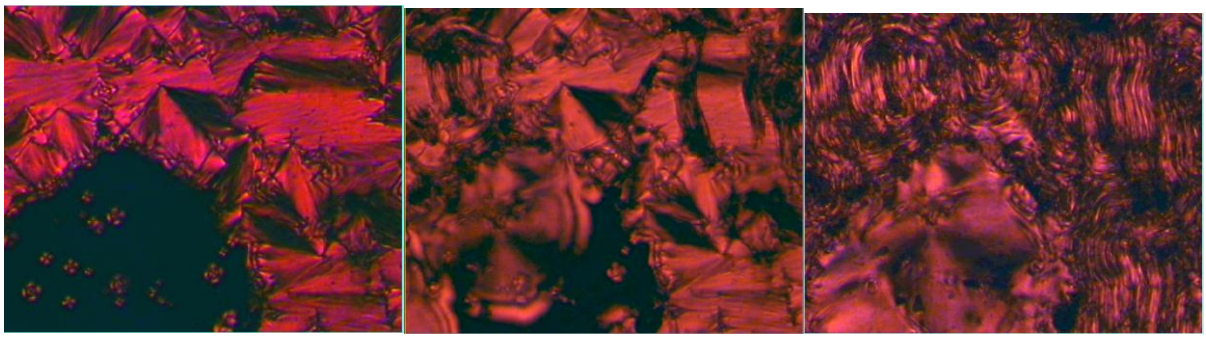

Supporting Figure 5. Optical polarising microscopy images showing the transition from SmA to SmC in compound **6-Zn(II)** on cooling from a) 130 °C, b) 110 °C and c) 92 °C.

6.0 X-ray Diffraction Experiments

6.1 High Temperature Smectic Phases

Temperature dependant X-ray diffraction was carried out for all compounds. Supporting figure 6 shows a representative 2D diffraction pattern for the cyanobiphenyl dimer compound **5** at low temperature.

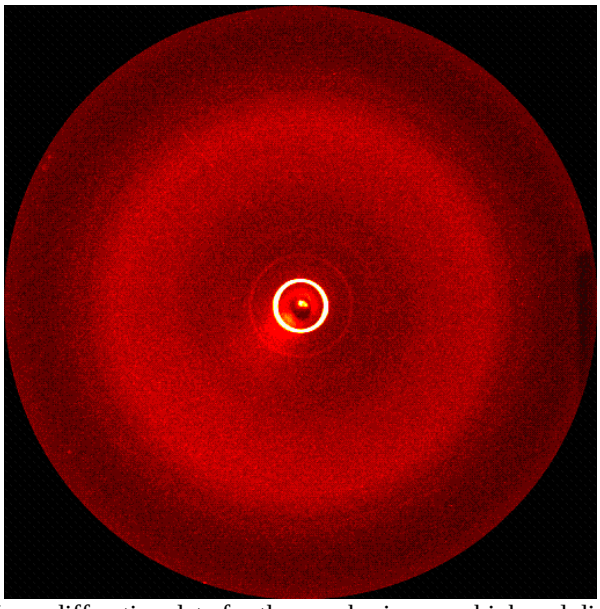

Supporting Figure 6. 2D X-ray diffraction data for the porphyrin cyanobiphenyl dimer.

Temperature dependant X-ray diffraction experiments were carried out at five degree intervals from room temperature to ten degrees above the isotropisation temperature identified by differential scanning calorimetry. The integrated X-ray diffraction patterns are shown below in Supporting Figure 7.

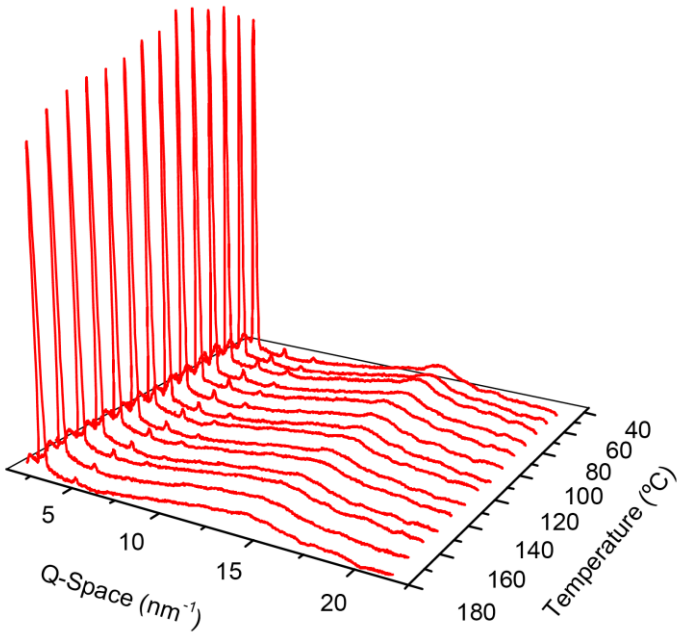

Supporting Figure 7. Integrated temperature dependant X-ray diffraction data.

Thermal optical polarizing microscopy experiments yielded clear focal conic texture in all high temperature phases indicative of a smectic A phase and although no preferential orientation could be obtained in the X-ray diffraction pattern, azimuthal integration shows no only minimal evidence of off meridian features (Supporting Figure 8).

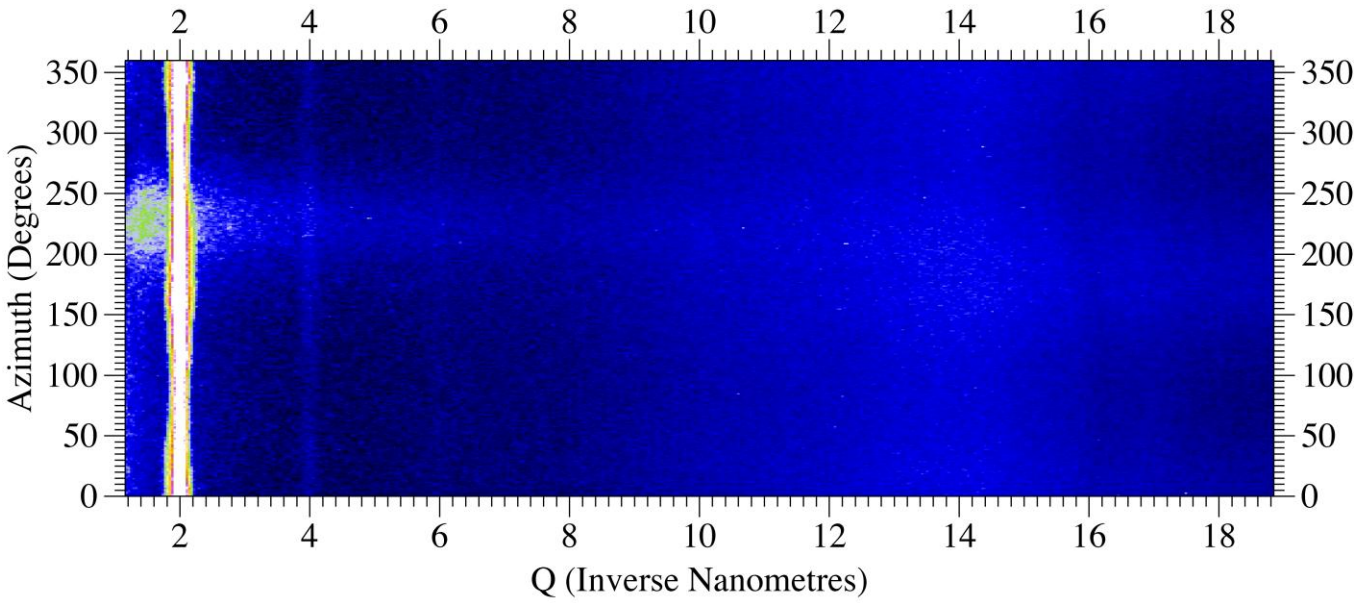

Supporting Figure 8. Azimuthal integration over the XRD pattern for compound 5.

6.2 X-ray Diffraction Data for Compound Zn(II)6

The low temperature smectic phase of **6-Zn(II)** observed by both optical polarising microscopy and DSC was investigated by X-ray diffraction experiments. Temperature dependant X-ray diffraction experiments carried out on the unsymmetric compound **Zn(II)6** are shown in Supporting Figure 9 the isotropic phase is indicated by the red line the high temperature smectic A phase is coloured orange. The mixed phase arising from partial transformation of the high temperature phase to a higher order phase is shown in yellow and the pure higher order phase is shown in green.

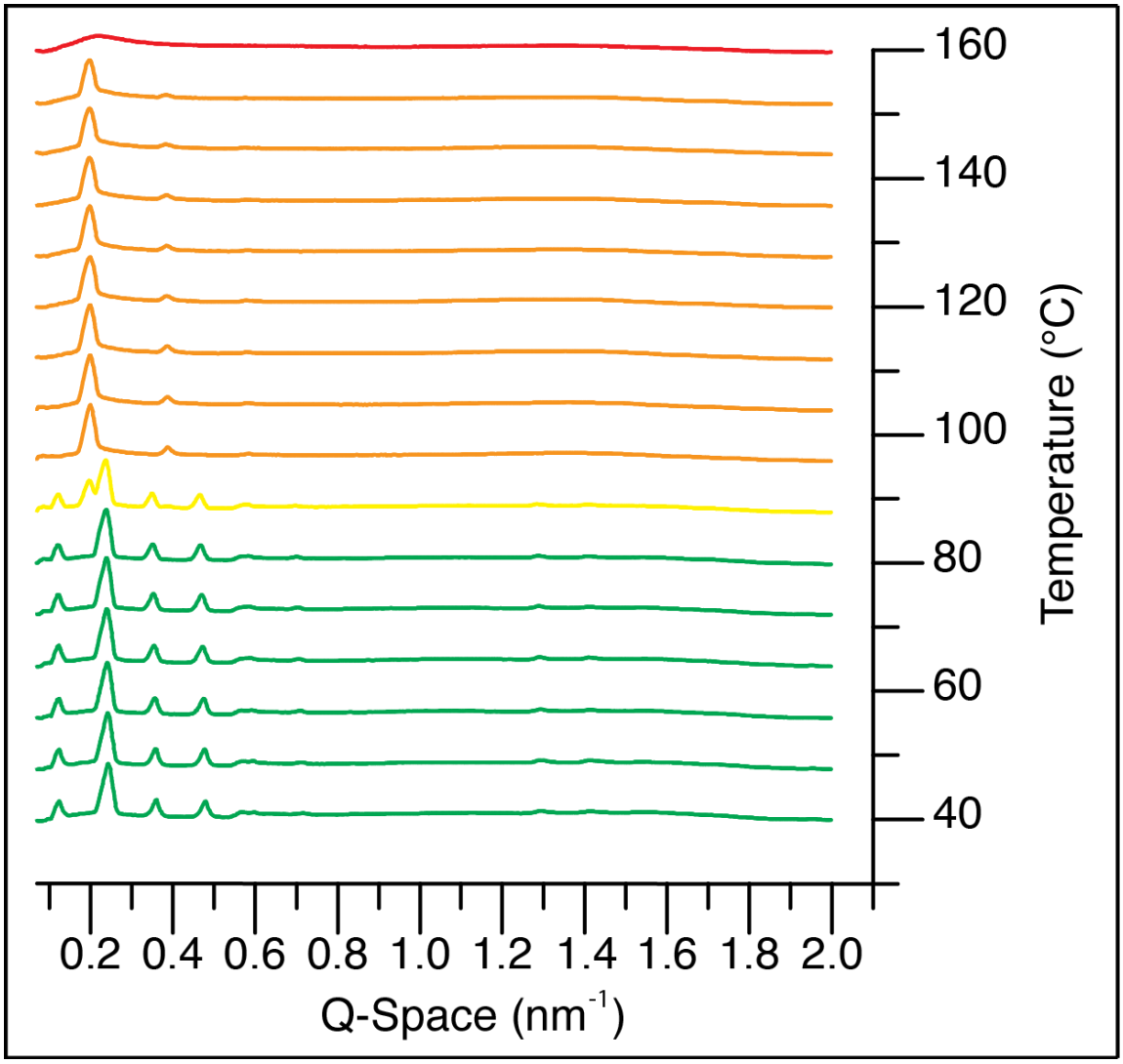

Supporting Figure 9. Integrated temperature dependant X-ray diffraction data for unsymmetric compound **Zn(II)6**.

At high temperature the compound shows similar diffraction patterns as for the remaining members of the series the integrated diffraction pattern at 120°C is shown in Supporting Figure 10.

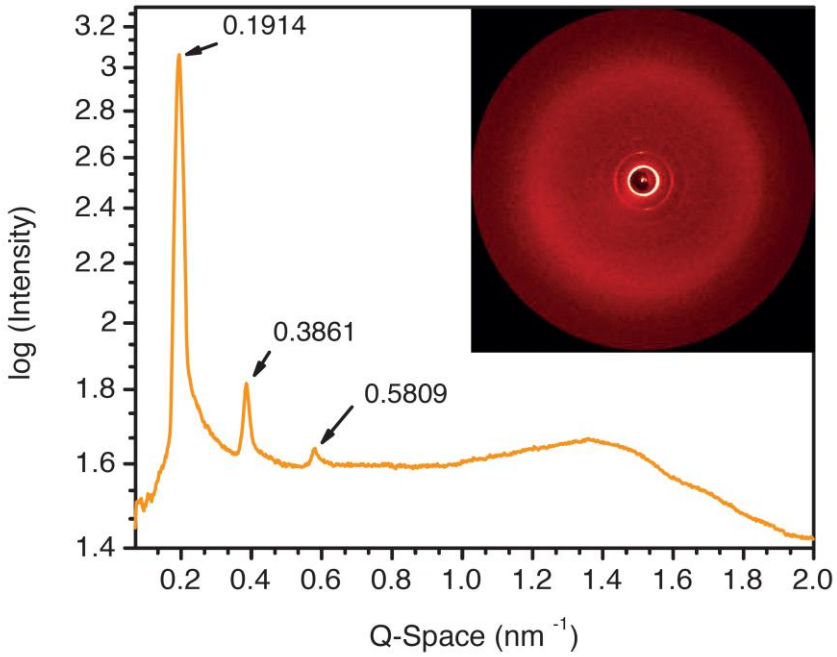

Supporting Figure 10. Integrated temperature dependant X-ray diffraction data for unsymmetric compound **Zn(II)6**.

Temperature dependent X-Ray diffraction experiments of the low temperature phase show the appearance of a lower intensity peak at q = 0.122 corresponding to a layer spacing of 51.5Å and a shift of the higher intensity peak previously assigned as the 01 peak in the higher temperature phase to wider angle Supporting Figure 11.

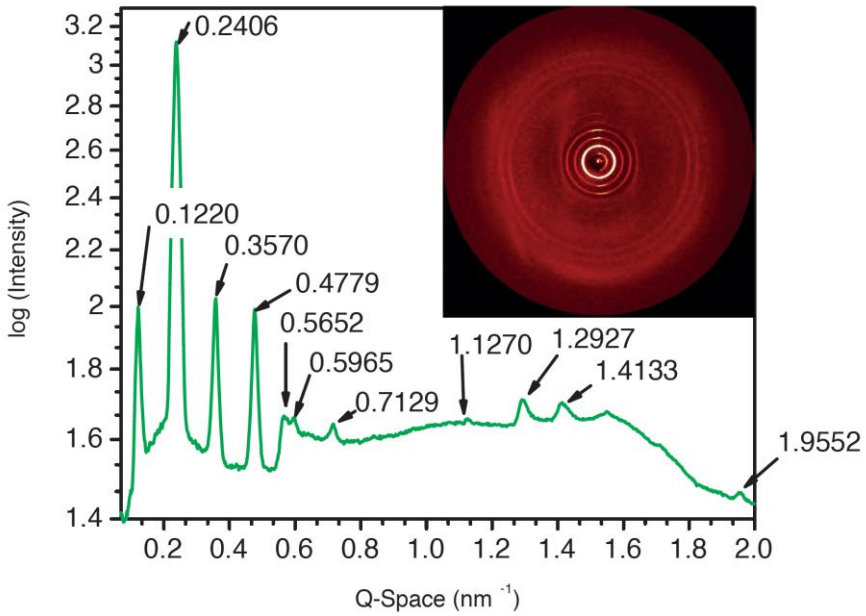

Supporting Figure 11. Integrated temperature dependant X-ray diffraction data for low temperature phase of unsymmetric compound **Zn(II)6**.

Indexing of the X-ray diffraction showed the presence of 01-06 peaks however a number of other peaks were observed which could not be indexed to a Sm A structure the comparative integrated X-ray diffraction patterns is shown below in Supporting Figure 12.

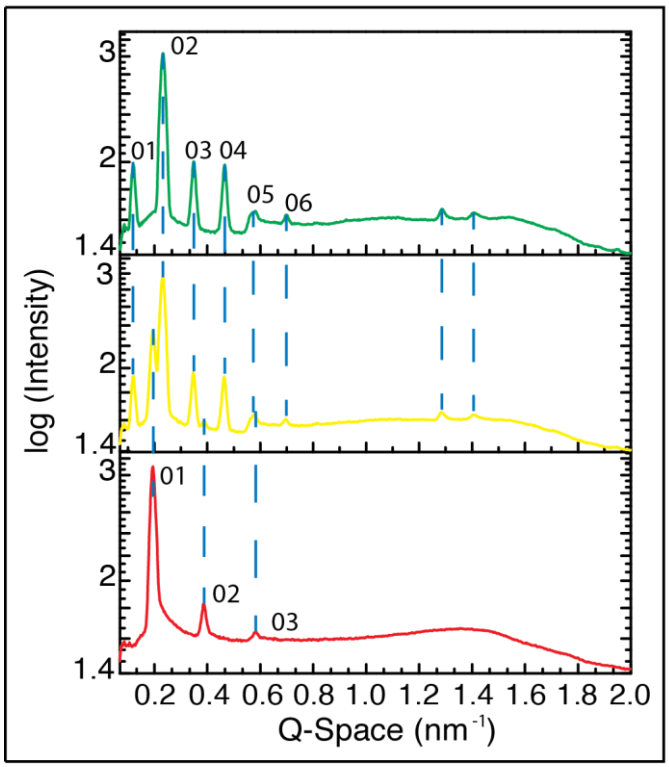

Supporting Figure 12. Integrated X-ray diffraction data for the low temperature high ordered phase (green) the mixed phase (yellow) and the high temperature SmA phase of unsymmetric compound **Zn(II)6**.

It was initially proposed that the addition of the metal ion and the single mesogen resulted in a higher ordered hexatic phase the additional peaks however are not consistent with this assignment, it is clear that the second phase represents a higher order phase. Combination of the additional peaks in the X-ray diffraction along with the OPM suggests the formation of a more ordered Smectic phase driven through restricted rotation of the porphyrin macrocycles within the smectic layers.

7.0 Reconstructed Electron Density Profiles

The electron density profile of a smectic liquid crystal assuming a centrosymmetric layer is described by a periodic function. The change in electron density from the average is represented as the cosine series according to equation 1. For a centrosymmetric layer the phase problem associated with reconstructing the electron density is reduced to the sign of the amplitudes of the X-ray diffraction data.

$$\Delta\rho(x) = \sum_{n=0}^{\infty} F_n cos\left(\frac{2\pi \cdot n \cdot x}{L}\right) \quad (1)$$

Δρ is the deviation of the electron density from the average, Fn is the amplitudes of the X-ray diffraction, n is the order of diffraction and L is the layer spacing. Three diffraction orders are visible and consequently the number of reconstructions are equal to $2^N = 2^3 = 8$. Four of these profiles are negatives of the others and therefore the number of reconstructions may be reduced to four.

To reconstruct the electron density profiles of the materials described herin background corrected experimental X-ray diffraction data was fitted to Lorentz functions using the least squares fitting processes available in the datasqueese software package. A representative fitting for compound 5 is shown below in Supporting Figures 13.

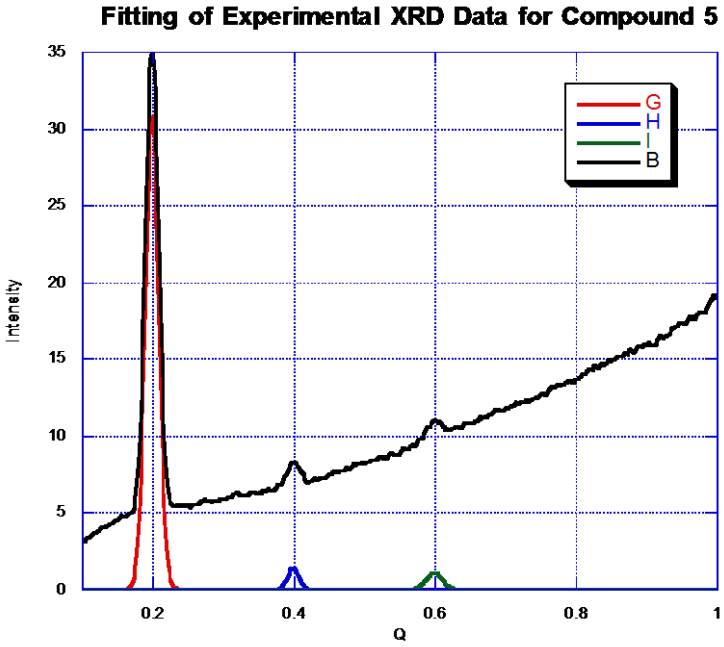

Supporting Figure 13. Lorentz fitted experimental X-ray diffraction data for compound 5.

The tabulated data for the fitting is shown below in Supporting Table 1 and the subsequent electron density solutions are shown in Supporting Figure 14.

Supporting Table 1. Lorentz corrected intensities for X-ray diffraction data for compound 5.

Peak	Q	Area	Intensity
001	0.199	3510.6	26.46
002	0.399	146.5	6.62
003	0.599	193.78	10.78

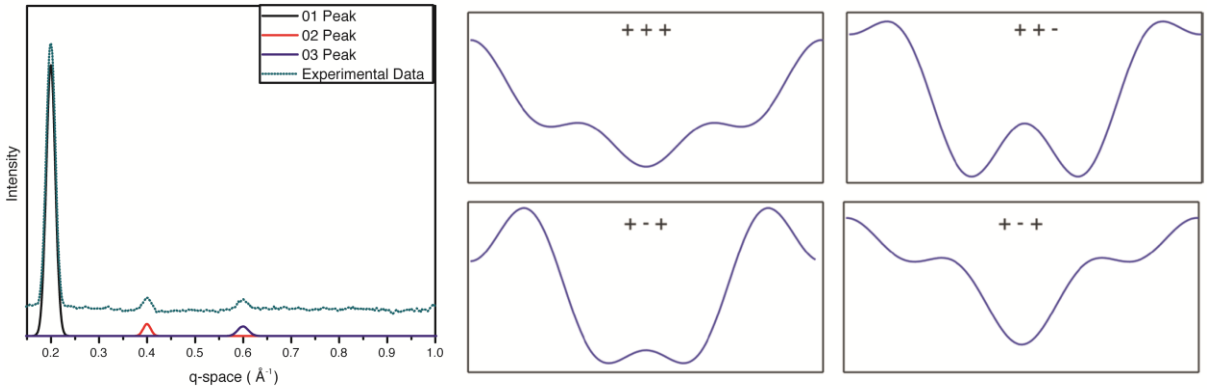

Supporting Figure 14. Reconstructed electron density profiles in the SmA phase of compound 5.

8.0 Molecular Modelling of LC Porphryins

The all trans molecular lengths for both the asymmetric and unsymmetric molecules were calculated using the PM3 algorithm in PCGamess (Supporting Figure 15). The lengths obtained were 68 and 91 Å respectively. These values are both significantly larger than the layer spacing observed experimentally.

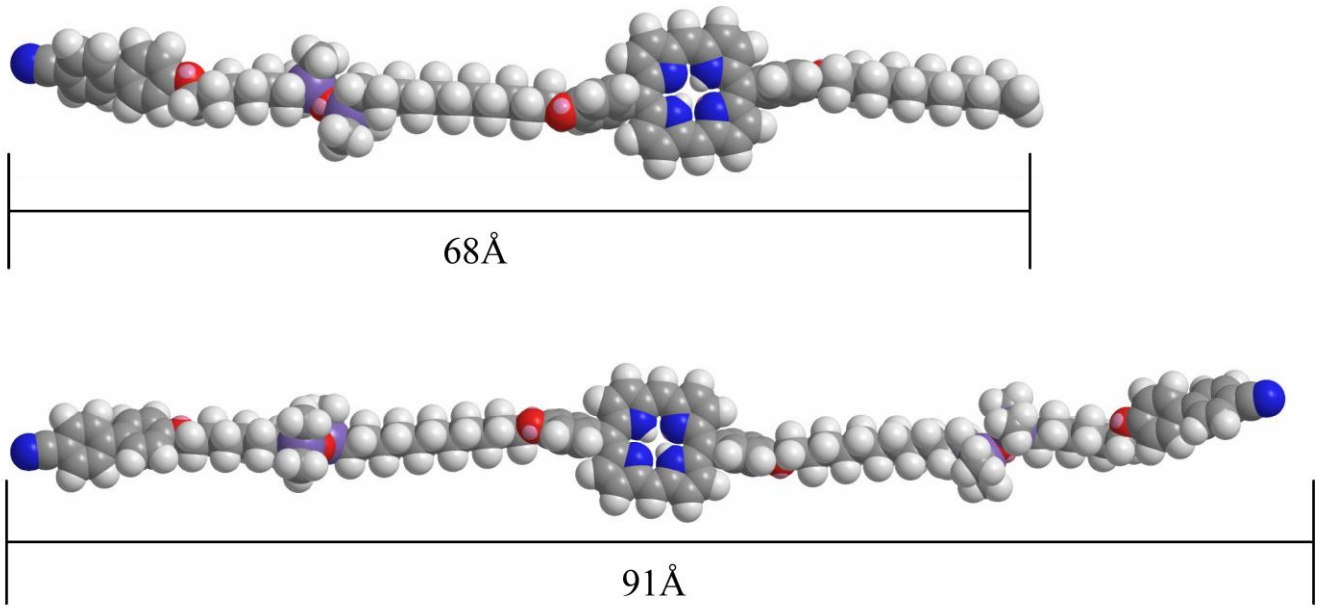

Supporting Figure 15. Fully Extended Molecular conformations of unsymmetrically and symmetrically substituted porphyrins.

In order to reconcile the molecular length to the layer spacing and subsequently elucidate potential packing models a number of conformations were investigated from the minimised structure incorporating various tilts and melting conformations of the alkyl chains. Molecular modelling of the aromatic portions of the molecules was carried out using PCGamess with the PM6 algorithm. The molecular dimensions are found below in Supporting Figure 14. The fully extended spacer length was calculated to be 24Å Supporting Figure 15. The chain contracted PM6 minimised structure is shown below in Supporting figure 16.

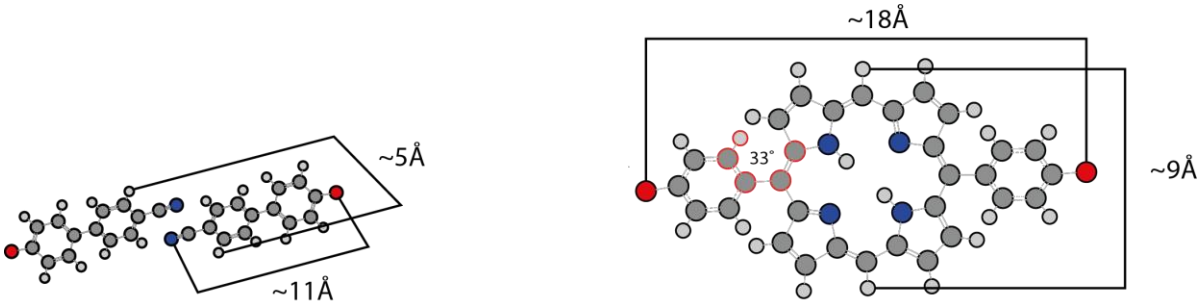

Supporting Figure 14. Molecular dimensions for aromatic segments calculated from PM6 minimisation.

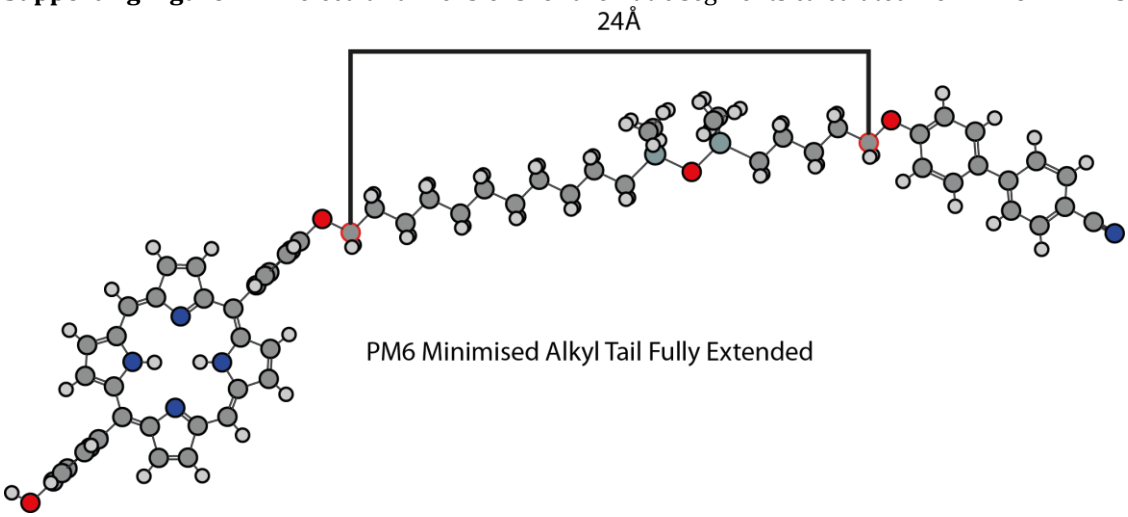

Supporting Figure 15. Fully extended all trans alkyl chain conformation PM6 minimisation (only half the molecule modelled to reduce computational overhead).

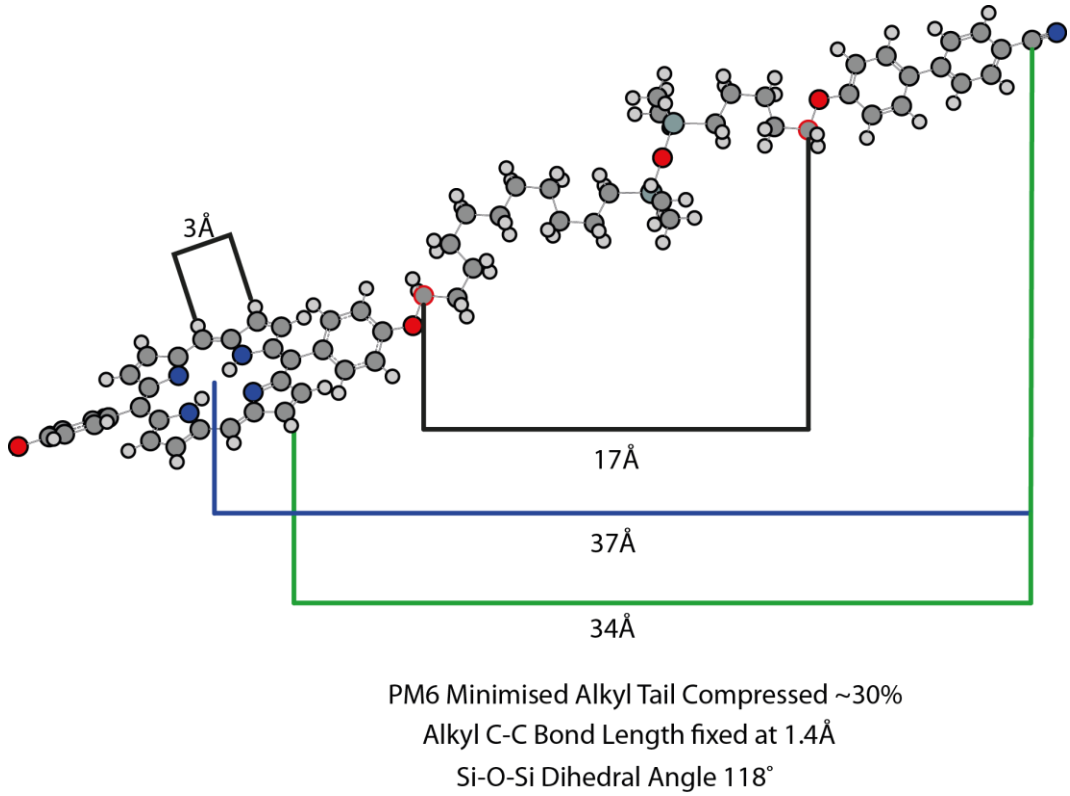

Supporting Figure 16. Chain contracted PM6 energy minimized model.

An assumption was made based on the centrosymmetric nature of the molecule that only ½ of the molecular length need to be encompassed by the unit cell of the lamellar phase thus the length of molecule that is required to pack into a 32 Å layer is ≈ 45 Å. By modifying the torsion angle of the phenyl-O-alkyl bond out of the plane of the porphryin ring at 105.3° a reduction in the molecular length of ~3Å which is equivalent to a molecular length contraction of ~7% was obtained however this does not provide sufficient apparent chain length reduction to fit half a molecule into a smectic layer. Alkyl chain contraction is well known in self-assembling dendrons and dendrimers and is indeed a prerequisite to satisfy the space filling requirements in most percec type dendritic systems. In order to provide a layer spacing encompassing half a molecule a contraction of the alkyl chains through the introduction of gauche conformations of 54% is required. When compared to some dendritic systems where chain contraction in the order of ~60% were observed this is a reasonable contraction parameter, however in the majority of smectic systems an all trans conformation is energetically more favourable. An alternative packing model may combine the out of plane rotation of the alkyl tails incorporating a limited number of gauche conformations along with a tilt of the alkyl chains will result in a similar reduction of the molecular length of ~50%.

9.0 Reconstructed Molecular Electron Density Profiles

To confirm the agreement of the proposed packing model with the reconstructed electron density the electron density profile for each model was approximated as a histogram by dividing the $0 < x < L$ range into discrete intervals (K) Δx. For the kth interval the electron density histogram was calculated according to Equation 2.

$$\rho_k \Delta x = \sum_j Z_{j,k} \quad (2)$$

Where the k^{th} interval is the summation over all atoms within the interval and Z is the atomic number. A three cell smooth was carried out according to Equation 3.

$$\rho'_k = \frac{1}{2}\left(\rho_k + \frac{\rho_{k-1} + \rho_{k+1}}{2}\right) \quad (3)$$

Three alternative models for a unit cell are shown below along with electron density histograms Supporting Figure 17. The first arrangement incorporates the parallel alignment of molecules within the layers and significant chain reduction via formation of multiple gauche conformations with cyannobiphenyl dimers formed by overlap with molecules from the adjacent layer. The second model is a modification of the first with the number of gauche conformations reduced by the formation of a Z shaped configuration of the molecule. The final model incorporates a head to tail arrangement of the molecules with each Porphyrin ring being eclipsed by a cyanobiphenyl dimer. In the final configuration a large number of gauche conformations are present in the chain however by increased overlap of the cyanobiphenyl groups these may be mitigated. The three packing models and electron density histograms presented are all in good agreement with the electron density profiles generated from the X-ray diffraction data in particular with the phase solutions ++- and +-+. Considering the observation that there is little change in the layer spacing morphology of the X-ray diffraction data between the symmetric and unsymmetric compounds bearing two and one cyannobiphenyl groups respectively it is most likely that the phase structure is dominated by the porphyrin macrocycle rather than the cyannobiphenyl units. This observation coupled with the significant in plane ordering discussed in the main body of the paper and the observation of correlations over 3 smectic layers in the X-ray diffraction pattern indicating that not only are molecules within the plane of the smectic layer correlated but that there is significant inter layer correlation it must be assumed that the phase structure is driven primarily by the self-assembly of porphyrin macrocycles with the formation of

cyannobipheyl dimers are a secondary driving force. Therefore although the model proposed in Supporting Figure 17c may be discounted and the most likely packing motif in the smectic phase being one of the solutions 17a or 17b however with the data available it is not possible to determine which of these packing models is the actual configuration within the smectic phase.

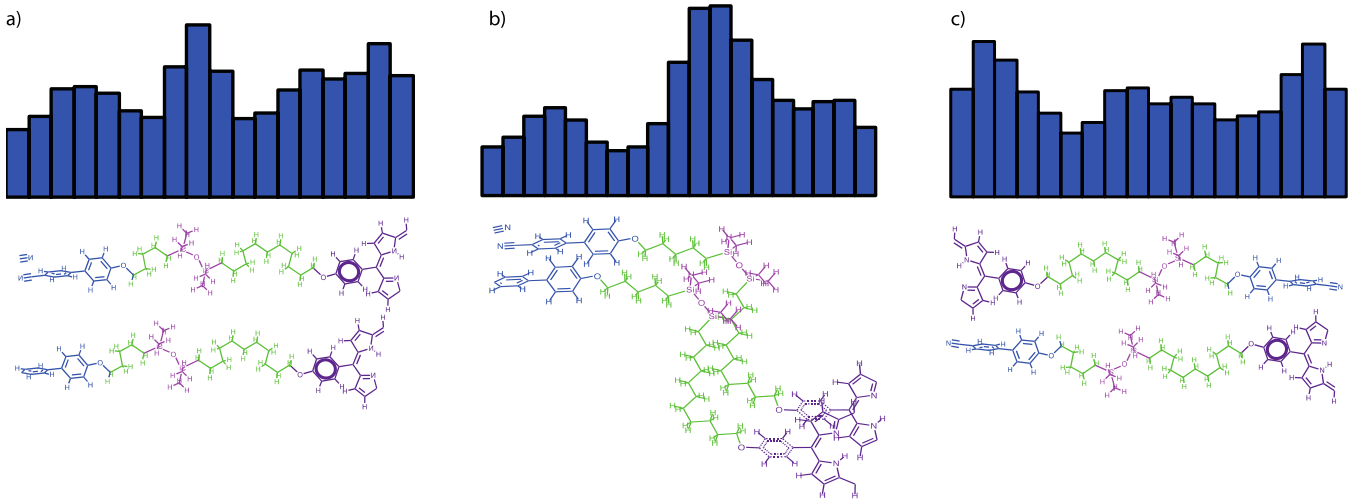

Supporting Figure 17. Electron density profiles for various molecular configurations.

(1) K. J Shepperson, T. Meyer, G. M. Mehl *Mol. Cryst. Liq. Cryst.* 2004, **411**, 1227-1233.